CHINESE OPTICS LETTERS

Vol. 21, No. 2 | February 2023

Spin-multiplexed full-space trifunctional terahertz metasurface [Invited]

Chuang Li (李 闯)[1], Shiwei Tang (汤世伟)[1*], Ziwei Zheng (郑紫微)[2], and Fei Ding (丁 飞)[3**]

[1] School of Physical Science and Technology, Ningbo University, Ningbo 315211, China

[2] Digital Industry Research Institute, Zhejiang Wanli University, Ningbo 315100, China

[3] Centre for Nano Optics, University of Southern Denmark, DK-5230 Odense M, Denmark

*Corresponding author: tangshiwei@nbu.edu.cn

**Corresponding author: feid@mci.sdu.dk

Received October 27, 2022 | Accepted January 3, 2023 | Posted Online February 27, 2023

The widespread use of multifunctional metasurfaces has started to revolutionize conventional electromagnetic devices due to their unprecedented capabilities and exceedingly low losses. Specifically, geometric metasurfaces that utilize spatially varied single-celled elements to impart arbitrary phase modulation under circularly polarized (CP) waves have attracted more attention. However, the geometric phase has intrinsically opposite signs for two spins, resulting in locked and mirrored functionalities for the right-handed and left-handed CP beams. Additionally, the demonstrated geometric metasurfaces so far have been limited to operating in either transmission or reflection modes at a single wavelength. Here, we propose a double-layered metasurface composed of complementary elliptical and reversal ring resonator structures to achieve simultaneous and independent control of the reflection and transmission of CP waves at two independent terahertz frequencies, which integrates three functions of reflected beam deflection, reflected Bessel beam generation, and transmitted beam focusing on the whole space. The high efficiency and simple design of our metasurface will open new avenues for integrated terahertz metadevices with advanced functionalities.

Keywords: terahertz metasurface; spin multiplexing; trifunction; full space; dual band.

DOI: 10.3788/COL202321.020002

1. Introduction

Metasurfaces, the counterpart of two-dimensional metamaterials[1], can arbitrarily manipulate the polarization, amplitude, and phase of the incident light in a subwavelength spatial resolution[2–4], and thus provide a good solution for realizing the integrated photonic metadevices with the advantages of miniaturization, integration, ease of fabrication, and multiple functionalities[5–7]. For instance, multifunctional geometric metasurfaces that integrated diversified functionalities for circularly polarized (CP) beams have been proposed by employing the segmented[8,9] or interleaved[10,11] configurations, resulting in unprecedented opportunities for the development of various integrated electromagnetic devices and systems. However, the segmented or interleaved metasurfaces intrinsically suffer from cross talk, low efficiency, and strict alignment requirements. Recently, by combining the resonance and the geometric phases in each meta-atom, spin-decoupled functionalities for two CP waves with suppressed cross talk and increased efficiency have been successfully implemented[12–14], such as multichannel metasurfaces[15–18], complex vector field generators[19,20], surface plasmon polariton metacouplers[21,22], spin-decoupled holograms[23], and spin-multiplexed optical imaging system[24,25].

A terahertz (THz) wave is generally defined as an electromagnetic wave with a frequency range of 0.1–10 THz, which is sandwiched between microwave and infrared radiation. It has the characteristics of high permeability, low energy, and a fingerprint spectrum. In recent years, with the development of physical technology and material science technology, the generation and detection methods of THz waves have become increasingly mature. The unique performance of THz waves has brought far-reaching influence on communication, radar, electronic countermeasure, electromagnetic weapons, astronomy, medical imaging, nondestructive testing, security inspection, and other fields. However, traditional materials are difficult to deal with THz waves, and their volume is huge, which seriously hinders the development of THz technology. The appearance of metasurfaces makes up for the absence of a THz-efficient manipulation device. Common electromagnetic wave control devices include focusing, imaging, wavefront shaping, and spin-multiplexed devices[26].

Despite the achievements in spin-multiplexed metasurfaces, the available functionalities are still limited. Additionally, they are often constrained to operating in either transmission or reflection modes at a single wavelength. In this paper, we propose a double-layered metasurface composed of two discrepant metallic layers separated by a polyimide spacer to achieve simultaneous and independent control of the reflected and transmitted CP waves at two independent THz frequencies. Capitalizing on the spin-decoupled concept, we realize three distinct functionalities (i.e., reflected beam deflection, reflected Bessel beam generation, and transmitted beam focusing) in the full space. The proposed method provides the possibility to realize high-efficiency multifunctional full-space electromagnetic devices at different frequencies, which may have important applications in the fields of wireless communication[27] and electromagnetic integration[28–31].

2. Meta-Atom Design

As schematically illustrated in Fig. 1(a), the proposed full-space trifunctional metasurface allows spin-controlled triple functionalities in the full space at two distinct frequencies. At the frequency f_1, spin-decoupled beam deflection and Bessel beam generation are realized for the right-handed circularly polarized (RCP) and left-handed circularly polarized (LCP) beams at normal incidence in the reflection mode. When the frequency is switched to f_2, the normally incident LCP light is converted into a focused RCP beam in transmission. Therefore, each meta-atom functions as a high-efficiency half-wave plate (HWP) in both reflection and transmission at f_1 and f_2, respectively, which is composed of two discrepant copper layers separated by a polyimide spacer, as shown in Figs. 1(b)–1(e). The upper and lower metallic layers both consist of internal and external parts, which guarantee the different phase responses at two frequencies without any cross talk. Specifically, the external split ring resonators (SRRs) and the inner complementary elliptical structures are used to control the phases of THz waves at the low and high frequencies, respectively. For instance, by properly adjusting the geometric parameters of the complementary elliptical structure, the meta-atom can meet the function of a reflective HWP at a specific frequency. At the same time, a high-performance transmissive HWP can be designed at another frequency by varying the SRRs without affecting the function of the reflective HWP. In the simulations, a low-loss polyimide spacer was selected to improve the transmission efficiency of CP THz waves, whose dielectric constant and loss tangent were set as 3.5 and 0.0027[32], respectively, while the copper was described as a lossy metal with a conductivity of $\sigma = 5.8 \times 10^7$ S/m.

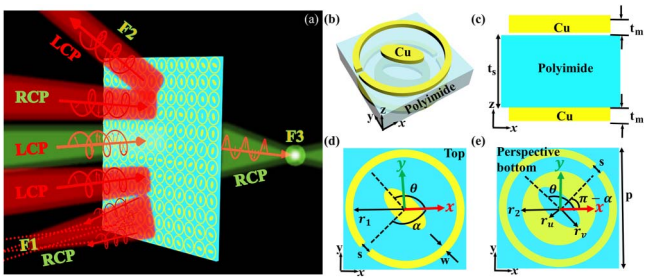

Fig. 1. (a) Schematic of the full-space trifunctional metasurface; (b), (c) perspective and side view of the meta-atom; (d), (e) top layer and bottom layer of the meta-atom. The dielectric substrate is polyimide (lossy) with a permittivity of 3.5 and a loss tangent of 0.0027, and the metallic part is copper with a conductivity of $\sigma = 5.8 \times 10^7$ S/m. The metallic layer of each meta-atom can be divided into inner and outer parts; the outer part consists of a reversed SRR structure, and the inner part consists of a complementary ellipse structure. The geometric parameters of the meta-atom are as follows: $p = 100$ μm, $t_s = 25$ μm, $t_m = 5$ μm, $r_v = 22$ μm, $r_u = 10$ μm, $r_1 = 43$ μm, $r_2 = 30$ μm, $w = 5$ μm, $s = 16$ μm.

The simulated reflection coefficients in the LP basis are shown in Fig. 2(a), where the reflection amplitudes are almost equal and the phase difference is roughly 180° at the frequency of 1.67 THz, indicating a highly efficient reflective HWP. As shown in Fig. 2(b), under the CP excitations at normal incidence, the designed meta-atom only reflects the co-polarized component, with $|r_{-+}|$ and $|r_{+-}|$ exceeding 0.9, while the cross-polarized counterparts (i.e., $|r_{++}|$ and $|r_{--}|$) are greatly suppressed at 1.67 THz. Besides the reflective HWP functionality, the designed meta-atom can serve as a transmissive HWP at the frequency of 0.51 THz. As shown in Fig. 2(d), the transmission amplitudes possess the same high levels under two LP excitations, whereas the transmission phase difference approaches 180°. Therefore, as shown in Fig. 2(e), the input CP beam is almost totally converted into its cross-polarized counterpart with the co-polarized component approaching 0 at 0.51 THz. In particular, the cross-polarized CP wave has a transmission amplitude as high as 0.88. To analyze the physical mechanism of high polarization conversion ratios in both reflection and transmission, we plotted the

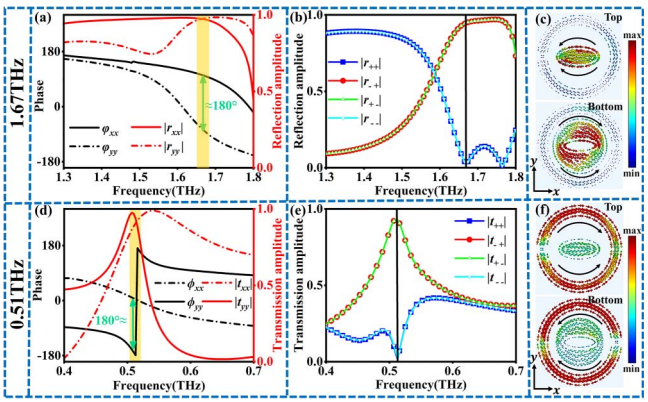

Fig. 2. Electromagnetic response of different meta-atoms. (a), (b) Reflection amplitudes and reflection phase under (a) LP and (b) CP waves at the frequency of 1.67 THz; (c) surface current distributions at the top and bottom copper layers under the LCP excitation at the frequency of 1.67 THz; (d), (e) transmission amplitudes and transmission phase under (d) LP and (e) CP waves at the frequency of 0.51 THz; (f) surface current distributions at the top and bottom copper layers under the LCP excitation at the frequency of 0.51 THz.

surface current distributions at the top and bottom copper layers [Figs. 2(c) and 2(f)]. As shown in Fig. 2(c), the complementary elliptical structures mainly respond to the electromagnetic wave at 1.67 THz, whereas the outer SRRs have negligible contributions. On the contrary, the SRRs dominate for the electromagnetic response at 0.51 THz, while the complementary elliptical structures have a minimal reaction. Impressively, the coupling between the complementary elliptical structures and SRRs is very weak, ensuring good performance at two distinct frequencies. As such, the geometric phase modulation for both the reflected and transmitted waves can be readily accomplished by rotating the resonator independently.

Through the above analysis, we have verified the HWP performance of the meta-atom, which makes it possible to make a spin-controlled full-space trifunctional metasurface. We use the Jones matrix to describe the electromagnetic properties of each meta-atom. In general, the rotated meta-atom that functions as a reflective HWP can be described by the matrix in the CP basis if we assume the reflection amplitudes under the x- and y-polarized excitations are equal ($|r_{xx}| = |r_{yy}|$)[33,34],

$$R_{\mathrm{CP}} = \begin{bmatrix} r_{++} & r_{+-} \\ r_{-+} & r_{--} \end{bmatrix} = \begin{bmatrix} 0 & |r_{xx}|e^{i(\varphi_{xx}-2\theta)} \\ |r_{xx}|e^{i(\varphi_{xx}+2\theta)} & 0 \end{bmatrix}, \quad (1)$$

where $|r_{xx}|$ and φ_{xx} are the reflection amplitude and phase of the meta-atoms under the x-polarized excitation, $|r_{yy}|$ is the reflection amplitude under the y-polarized excitation, θ is the rotation angle of the complementary elliptical structure, and r_{-+}, r_{--}, r_{++}, and r_{+-} represent the complex reflection coefficients in the CP basis, with the first subscript indicating the polarization state of the reflected wave and the second indicating the polarization state of the incident wave. Here the subscripts "+" and "−" indicate that the time-animated field vector is rotating according to the left- and right-handed orientation when looking into the incident direction of the negative z axis. For the incident wave and the transmitted wave propagating along the negative z axis, "+" and "−" correspond to LCP and RCP, respectively. But for the reflected wave propagating along the positive z axis, "+" and "−" correspond to RCP and LCP, respectively. Therefore, the co-polarized CP components of r_{-+} and r_{+-} include geometric phase term $\pm 2\theta$ and resonant phase term φ_{xx}. The geometric phase is effectively modulated by the rotation of the meta-atom, and the resonance phase term provides extra degrees of freedom to decouple the phases of r_{-+} and r_{+-}, thereby resulting in spin-decoupled functionalities in reflection. Similarly, the transmissive HWP meta-atom can be described by the Jones matrix T_{CP},

$$T_{\mathrm{CP}} = \begin{bmatrix} t_{++} & t_{+-} \\ t_{-+} & t_{--} \end{bmatrix} = \begin{bmatrix} 0 & |t_{xx}|e^{i(\phi_{xx}-2\alpha)} \\ |t_{xx}|e^{i(\phi_{xx}+2\alpha)} & 0 \end{bmatrix}, \quad (2)$$

where α is the rotation angle of SRRs, t_{++}, t_{+-}, t_{-+}, and t_{--} represent the complex transmission coefficients of CP waves, and $|t_{xx}|$ and ϕ_{xx}, respectively, represent the transmission amplitude and phase under the x-polarized wave excitation.

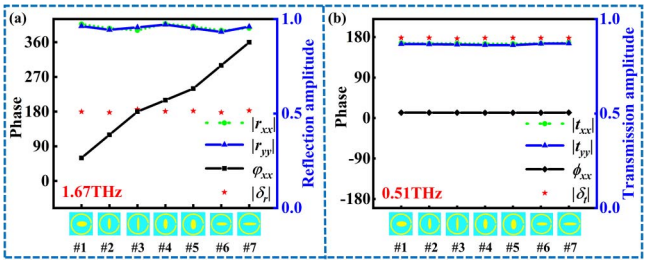

Fig. 3. (a) Reflection amplitudes, phases, and phase difference of the seven meta-atoms comprising the subarray under LP waves at the frequency of 1.67 THz; (b) transmission amplitudes, phases, and phase difference of the seven meta-atoms comprising the subarray under LP waves at the frequency of 0.51 THz.

Therefore, multiple efficient HWPs with wide resonance phase φ_{xx} (ϕ_{xx}) coverages are required to realize spin-multiplexed phase control over the reflected or transmitted fields simultaneously. To simplify the design and validate our design, we utilize both the resonance and geometric phases to decouple the phase profiles for the reflected fields at 1.67 THz, while only the geometric phase is used for the transmitted wave at the frequency of 0.51 THz. Figure 3 shows the electromagnetic response of the designed HWP meta-atoms under the LCP excitation at two different frequencies. Seven anisotropic HWP meta-atoms covering the 2π phase range are selected to form a subarray for polarization rotation and phase manipulation. Impressively, all HWPs maintain high efficiencies with both reflection and transmission amplitudes larger than 0.9 and 0.88 at the frequencies of 1.67 and 0.51 THz, respectively. At the same time, the change of the complementary elliptical structure does not affect the high transmission amplitudes at 0.51 THz. Additionally, the reflection phase difference $\delta_r = |\varphi_{xx} - \varphi_{yy}|$ at 1.67 THz and transmission phase difference $\delta_t = |\phi_{xx} - \phi_{yy}|$ at 0.51 THz are maintained at ∼180°, ensuring good HWP functionalities.

3. Full-Space Trifunctional Metasurface

Based on the meta-atom library, we design a spin-controlled trifunctional metasurface by arranging the appropriate meta-atoms in a one-dimensional (1D) supercell. The 1D supercell is composed of 24 meta-atoms with an overall size of 100 μm × 2400 μm. Under the excitation of CP waves, three different functionalities (i.e., reflected beam deflection, reflected Bessel beam generation, and transmitted beam focusing) are realized simultaneously at different frequencies.

To realize the full-space trifunctional metasurface for both RCP and LCP incident waves, both the resonance and geometric phases are utilized to fulfill the following condition[35–37]:

$$\varphi_{xx} + 2\theta = \varphi_{f1-+} = \frac{2\pi}{np}|x| + \varphi_0, \quad (3)$$

$$\varphi_{xx} - 2\theta = \varphi_{f1+-} = \frac{2\pi}{np}x + \varphi_0, \quad (4)$$

$$2\alpha = \varphi_{f2} = \frac{2\pi}{\lambda_2}\left(\sqrt{x^2 + F^2} - F\right), \tag{5}$$

where φ_{f1-+} and φ_{f1+-} indicate the phase distributions of the co-polarized reflected waves under the LCP and RCP excitations, $n = 6$ is the number of meta-atoms enabling the 2π phase coverage, p is the periodicity of the meta-atoms along the x-axis direction, φ_0 is the constant initial phase, φ_{f2} is the 1D hyperbolic phase for the focusing lens, and $F = 800$ μm is the focal length. Figure 4 displays the resonance and geometric phase distributions of all 24 meta-atoms comprising a supercell under two CP beams at two different frequencies, where the resonance phase φ_{xx} has equal contributions for both spins, while the geometric phase $\pm 2\theta$ has opposite contributions. Since the designed HWP meta-atoms have no resonance phase variation for the transmitted field at 0.51 THz, only the geometric phase contributes to the phase modulation and eventually the wavefront shaping in transmission.

According to the phase distributions in Fig. 4, the full-space metasurface can be realized by selecting and arranging the proper meta-atoms. When LCP waves are incident on the metasurface at 1.67 THz, the reflected beam will maintain its polarization state and form a Bessel beam [Fig. 5(a)]. Figure 5(b) shows the electric field distribution in the reflection side at the frequency of 1.67 THz, indicating the nondiffraction feature. To check the quality of the generated Bessel beam, we also map out the intensity distribution along the propagation direction. From Fig. 5(c), we can find that the Bessel beam has a depth of focus of 1900 μm, which is close to the theoretical value $\frac{np}{\tan\theta_L} \approx 1908.7$ μm. Figure 5(d) shows the intensity along a horizontal cut across the centers of Fig. 5(c), where the calculated full width at half-maximum (FWHM) is found to be 236 μm, in good agreement with the theoretical value of 231 μm.

When the incident beam is switched to the RCP state, the reflected light maintains its spin and is deflected to an anomalous angle, as shown in Fig. 6(a). Figure 6(b) shows the electric

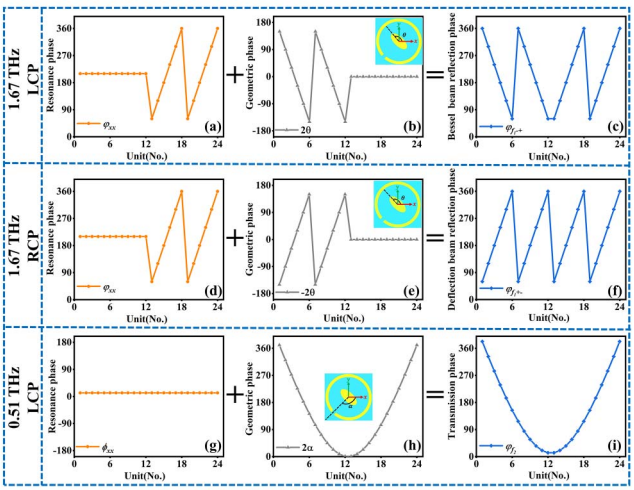

Fig. 4. (a)–(c) Under the LCP excitation at the frequency of 1.67 THz, the resonant, geometric, and total phase distributions of the meta-atoms for the reflected Bessel beam; (d)–(f) under the RCP excitation at the frequency of 1.67 THz, the resonant, geometric, and total phase distributions of the meta-atoms for the reflected beam deflection; (g)–(i) under the LCP excitation at the frequency of 0.51 THz, the resonant, geometric, and total phase distributions for the meta-atoms of the transmitted beam focusing.

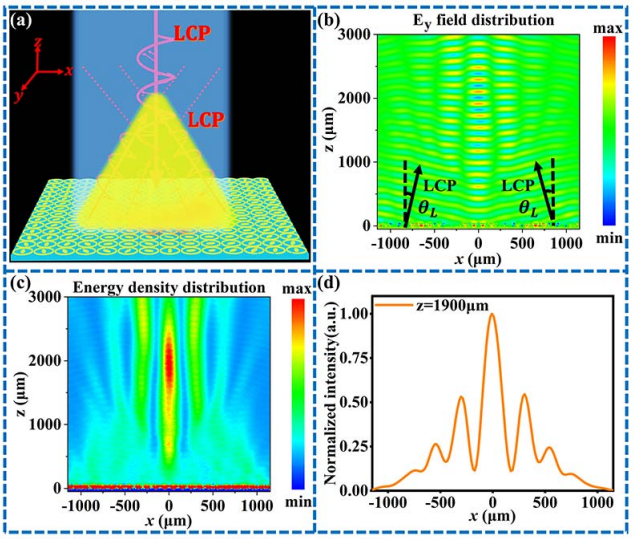

Fig. 5. Reflected Bessel beam generation under the LCP excitation at the frequency of 1.67 THz. (a) Schematic diagram of the Bessel beam generation under the LCP excitation; (b) electric field E_y distribution on the *xoz* plane under the LCP excitation; (c) intensity distribution on the *xoz* plane under the LCP excitation; (d) normalized intensity profile along a horizontal cut at $z = 1900$ μm.

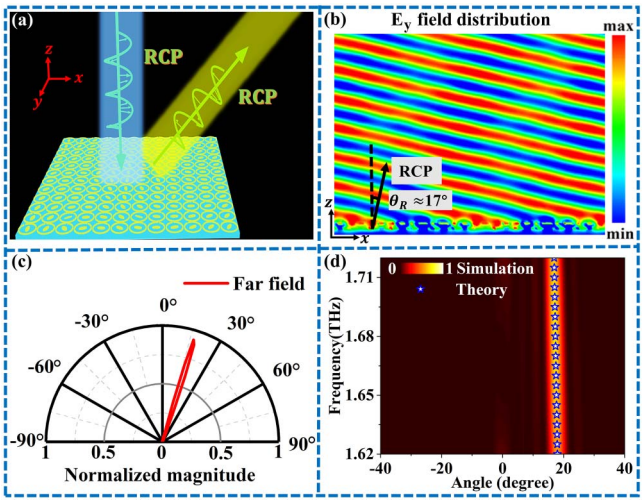

Fig. 6. Reflected beam deflection under the RCP excitation at the frequency of 1.67 THz. (a) Schematic diagram of the beam deflection under the RCP excitation; (b) electric field E_y distribution on the *xoz* plane under the RCP excitation; (c) far-field polar plot under the RCP excitation at 1.67 THz; (d) far-field intensity distribution as a function of the frequency and polar angle under the RCP excitation; the red color column is simulated, while the blue color star is theoretical, representing the simulated and theoretically predicted deflection angles, respectively.

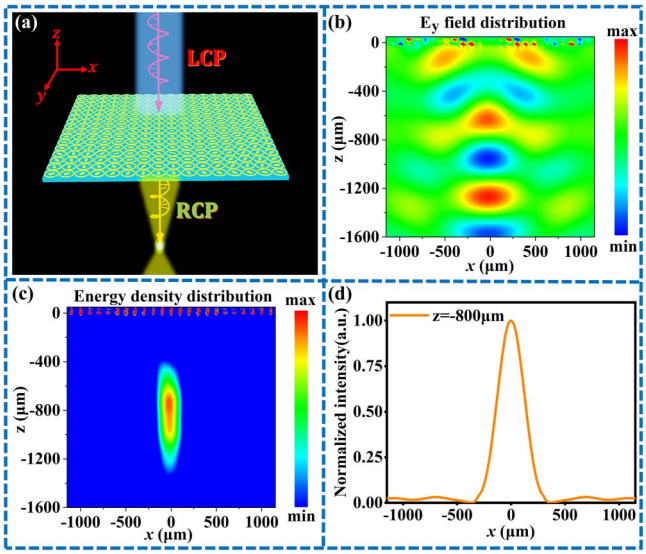

Fig. 7. Transmitted beam focusing under the LCP excitation at the frequency of 0.51 THz. (a) Schematic of the focusing lens at 0.51 THz; (b) electric field E_y distribution on *xoz* plane under the LCP excitation; (c) intensity distribution on the *xoz* plane under the LCP excitation; (d) normalized intensity profile along a horizontal cut at $z = -800$ μm.

field distribution of the deflected beam at the designed frequency of 1.67 THz, indicating that the front edge of the reflected wave is inclined, which is in good agreement with the far-field plot [Fig. 6(c)]. Besides the designed frequency, the metasurface can achieve beam deflection in a frequency range from 1.62 to 1.72 THz, where the deflection angle can be well described by the generalized Snell's law $\theta_R = \arcsin(\frac{2\pi}{npk_0})$ [blue dashed five-pointed stars in Fig. 6(d)].

In addition to the reflection mode, the designed metasurface can work as a focusing lens at another frequency, 0.51 THz. As shown in Fig. 7(a), the LCP incident wave is converted into the RCP-focused wave passing through the metasurface. The electric field and intensity distributions of the focused beam are shown in Figs. 7(b) and 7(c), indicating clearly that the incoming plane wave is slightly focused with a focal length of 800 μm, which is identified from the maximum-intensity position along the z axis. The calculated FWHM is around 326 μm, demonstrating the diffraction-limited focusing property.

4. Conclusion

We have combined the concepts of spin-decoupling and frequency-multiplexing to realize a spin-controlled THz metasurface that enables three distinct functionalities in the whole space. Capitalizing on the properly designed double-layered meta-atoms that can independently control the reflected and transmitted CP waves at two separate THz frequencies, maintaining excellent efficiency, reflected beam deflection, reflected Bessel beam generation, and transmitted beam focusing have been accordingly demonstrated. The proposed full-space metasurface exhibits the advantages of simple design, low cross talk, and high efficiency, which may expand the scope of electromagnetic manipulation and accelerate the integration of electromagnetic components and systems with advanced functionalities.

Acknowledgement

This work was supported by the Villum Fonden (No. 37372), Independent Research Fund Denmark (No. 1134-00010B), Natural Science Foundation of Zhejiang Province (No. LY19A040004), and Natural Science Foundation of Ningbo (No. 2021J073).

References

1. R. Ji, K. Song, X. Guo, X. Xie, Y. Zhao, C. Jin, S. Wang, C. Jiang, J. Yin, Y. Liu, S. Zhai, X. Zhao, and W. Lu, "Spin-decoupled metasurface for broadband and pixel-saving polarization rotation and wavefront control," Opt. Express **29**, 25720 (2021).
2. L. Chen, T. Ren, Y. Zhao, Q. Yu, Z. Huang, K. Zhang, J. Wen, F. Lin, and S. Chen, "Polarization-independent wavefront manipulation of surface plasmons with plasmonic metasurfaces," Adv. Opt. Mater. **8**, 2000868 (2020).
3. Z. Cheng and Y. Cheng, "A multi-functional polarization convertor based on chiral metamaterial for terahertz waves," Opt. Commun. **435**, 178 (2018).
4. H. Li, G. Wang, L. Zhu, X. Gao, and H. Hou, "Wideband beam-forming metasurface with simultaneous phase and amplitude modulation," Opt. Commun. **466**, 124601 (2020).
5. W. Xiao and C. Huang, "Highly-efficient wavefront bending with a single-layer perforated metasurface," J. Opt. **23**, 25103 (2021).
6. S. Q. Tang, K. H. H. Li, S. J. Lee, J. J. Zeng, and S. H. Ng, "Novel multi-way microvalve with ease of fabrication and integration for microfluidics application," Sens. Actuators B Chem. **286**, 289 (2019).
7. H.-X. Xu, M. Wang, G. Hu, S. Wang, Y. Wang, C. Wang, Y. Zeng, J. Li, S. Zhang, and W. Huang, "Adaptable invisibility management using kirigami-inspired transformable metamaterials," Research **2021**, 9806789 (2021).
8. S. Liu, L. Zhang, Q. L. Yang, Q. Xu, Y. Yang, A. Noor, Q. Zhang, S. Iqbal, X. Wan, Z. Tian, W. X. Tang, Q. Cheng, J. G. Han, W. L. Zhang, and T. J. Cui, "Frequency-dependent dual-functional coding metasurfaces at terahertz frequencies," Adv. Opt. Mater. **4**, 1965 (2016).
9. R. Amin and G. Anthony, "Broadband, multiband, and multifunctional all-dielectric metasurfaces," Phys. Rev. Appl. **11**, 054066 (2019).
10. A. Vallecchi, R. J. Langley, and A. G. Schuchinsky, "Metasurfaces with interleaved conductors: phenomenology and applications to frequency selective and high impedance surfaces," IEEE Trans. Antennas Propag. **64**, 599 (2016).
11. P. Ratanak and L. Sungjoon, "Dynamically self-reconfigurable multifunctional all-passive metasurface," ACS Appl. Mater. Interfaces **12**, 42393 (2020).
12. Y. Guo, S. Zhang, M. Pu, Q. He, J. Jin, M. Xu, Y. Zhang, P. Gao, and X. Luo, "Spin-decoupled metasurface for simultaneous detection of spin and orbital angular momenta via momentum transformation," Light Sci. Appl. **10**, 63 (2021).
13. Q. Zhang, R. Xie, Z. Gu, H. Zhang, C. Chen, J. Ding, and W. Chen, "Broadband high-efficiency polarization-encoded meta-holograms based on 3-bit spin-decoupled reflective meta-atoms," Opt. Express **30**, 4249 (2022).
14. H. X. Xu, Y. Wang, C. Wang, M. Wang, S. Wang, F. Ding, Y. Huang, X. Zhang, H. Liu, X. Ling, and W. Huang, "Deterministic approach to achieve full-polarization cloak," Research **2021**, 6382172 (2021).
15. C. Zhang, F. Dong, Y. Intaravanne, X. Zang, L. Xu, Z. Song, G. Zheng, W. Wang, W. Chu, and X. Chen, "Multichannel metasurfaces for anticounterfeiting," Phys. Rev. Appl. **12**, 34028 (2019).
16. F. F. Qin, Z. Z. Liu, Z. Zhang, Q. Zhang, and J. J. Xiao, "Broadband full-color multichannel hologram with geometric metasurface," Opt. Express **26**, 11577 (2018).

17. H. X. Xu, C. Wang, G. Hu, Y. Wang, S. Tang, Y. Huang, X. Ling, W. Huang, and C. W. Qiu, "Spin-encoded wavelength-direction multitasking Janus metasurfaces," Adv. Opt. Mater. **9**, 2100190 (2021).
18. H. X. Xu, G. Hu, M. Jiang, S. Tang, Y. Wang, C. Wang, Y. Huang, X. Ling, H. Liu, and J. Zhou, "Wavevector and frequency multiplexing performed by a spin-decoupled multichannel metasurface," Adv. Mater. Technol. **5**, 1900710 (2020).
19. D. Wang, T. Liu, Y. Zhou, X. Zheng, S. Sun, Q. He, and L. Zhou, "High-efficiency metadevices for bifunctional generations of vectorial optical fields," Nanophotonics **10**, 685 (2020).
20. W. Han, Y. Yang, W. Cheng, and Q. Zhan, "Vectorial optical field generator for the creation of arbitrarily complex fields," Opt. Express **21**, 20695 (2013).
21. D. Wang, K. Liu, X. Li, G. Wang, S. Tang, and T. Cai, "Bifunctional spoof surface plasmon polariton meta-coupler using anisotropic transmissive metasurface," Nanophotonics **11**, 1177 (2022).
22. X. Ye, H. Liu, Y. Qiao, and X. Chen, "Enhancement of surface plasmon polariton excitation via feedback-based wavefront shaping," Opt. Lett. **43**, 6021 (2018).
23. C. Chen, S. Gao, W. Song, H. Li, S. Zhu, and T. Li, "Metasurfaces with planar chiral meta-atoms for spin light manipulation," Nano Lett. **21**, 1815 (2021).
24. Y. Fu, C. Min, J. Yu, Z. Xie, G. Si, X. Wang, Y. Zhang, T. Lei, J. Lin, D. Wang, H. P. Urbach, and X. Yuan, "Measuring phase and polarization singularities of light using spin-multiplexing metasurfaces," Nanoscale **11**, 18303 (2019).
25. H.-X. Xu, G. Hu, Y. Li, L. Han, J. Zhao, Y. Sun, F. Yuan, G.-M. Wang, Z. H. Jiang, X. Ling, T. J. Cui, and C.-W. Qiu, "Interference-assisted kaleidoscopic meta-plexer for arbitrary spin-wavefront manipulation," Light Sci. Appl. **8**, 3 (2019).
26. J. He, X. He, T. Dong, S. Wang, M. Fu, and Y. Zhang, "Recent progress and applications of terahertz metamaterials," J. Phys. D **55**, 123002 (2022).
27. X. Zhang, Y. Sun, B. Zhu, W. Jiang, Q. Yu, H. Tian, C. Qiu, Z. Zhang, and T. Cui, "A metasurface-based light-to-microwave transmitter for hybrid wireless communications," Light Sci. Appl. **11**, 126 (2022).
28. H. Chu, Q. Li, B. Liu, J. Luo, S. Sun, Z. H. Hang, L. Zhou, and Y. Lai, "A hybrid invisibility cloak based on integration of transparent metasurfaces and zero-index materials," Light Sci. Appl. **7**, 50 (2018).
29. Y. Li, S. Wang, H. Wang, H. Li, J. Shen, and T. Cui, "Nonreciprocal control of electromagnetic polarizations applying active metasurfaces," Adv. Opt. Mater. **10**, 2102154 (2022).
30. L. Wu, Q. Xiao, Y. Gou, R. Wu, P. Xu, Y. Qing, Z. Wang, L. Bao, H. Ma, and T. Cui, "Electromagnetic diffusion and encryption holography integration based on reflection–transmission reconfigurable digital coding metasurface," Adv. Opt. Mater. **10**, 2102657 (2022).
31. H. X. Xu, L. Han, Y. Li, Y. Yan, J. Zhao, S. Zhang, and C. W. Qiu, "Completely spin-decoupled dual-phase hybrid metasurfaces for arbitrary wavefront control," ACS Photonics **6**, 211 (2019).
32. J. Fan, Y. Cheng, and B. He, "High-efficiency ultrathin terahertz geometric metasurface for full-space wavefront manipulation at two frequencies," J. Phys. D **54**, 115101 (2021).
33. C. Meng, S. Tang, F. Ding, and S. I. Bozhevolnyi, "Optical gap-surface plasmon metasurfaces for spin-controlled surface plasmon excitation and anomalous beam steering," ACS Photonics **7**, 1849 (2020).
34. Q. Fan, M. Liu, C. Zhang, W. Zhu, Y. Wang, P. Lin, F. Yan, L. Chen, H. J. Lezec, Y. Lu, A. Agrawal, and T. Xu, "Independent amplitude control of arbitrary orthogonal states of polarization via dielectric metasurfaces," Phys. Rev. Lett. **125**, 267402 (2020).
35. S. Tang, X. Li, W. Pan, J. Zhou, T. Jiang, and F. Ding, "High-efficiency broadband vortex beam generator based on transmissive metasurface," Opt. Express **27**, 4281 (2019).
36. F. Ding, B. Chang, Q. Wei, L. Huang, X. Guan, and S. I. Bozhevolnyi, "Versatile polarization generation and manipulation using dielectric metasurfaces," Laser Photonics Rev. **14**, 2000116 (2020).
37. Y. Xu, Q. Li, X. Zhang, M. Wei, Q. Xu, Q. Wang, H. Zhang, W. Zhang, C. Hu, Z. Zhang, C. Zhang, X. Zhang, J. Han, and W. Zhang, "Spin-decoupled multifunctional metasurface for asymmetric polarization generation," ACS Photonics **6**, 2933 (2019).